



# Hyperfoams: Energy dissipation and shock wave formation

Vladimir Bratov and Sergey V. Kuznetsov

**Abstract.** It has been found that highly porous organic foams (hyperfoams) modeled by the Blatz–Ko and Hill hyperelastic potentials may exhibit mechanical energy loss caused by the formation and propagation of strain discontinuities arising when a portion of a faster wave pulse overtakes a slower one. This observation opens up a possibility for creating a new type of shock absorbers containing no viscous or dry friction elements. For example, the considered Blatz–Ko-type hyperelastic potential is a good material behavior model for moderately stiff polyurethane (PU) foams both at large compression and at large extension strains. The analysis utilizes a combined method consisting of the explicit time integration technique coupled with the finite element method for spatial discretization.

**Mathematics Subject Classification.** 74J40.

**Keywords.** Hyperfoam, Shock absorber, Shock wave front, Blatz–Ko potential, Acoustic wave, Energy dissipation.

## 1. Introduction

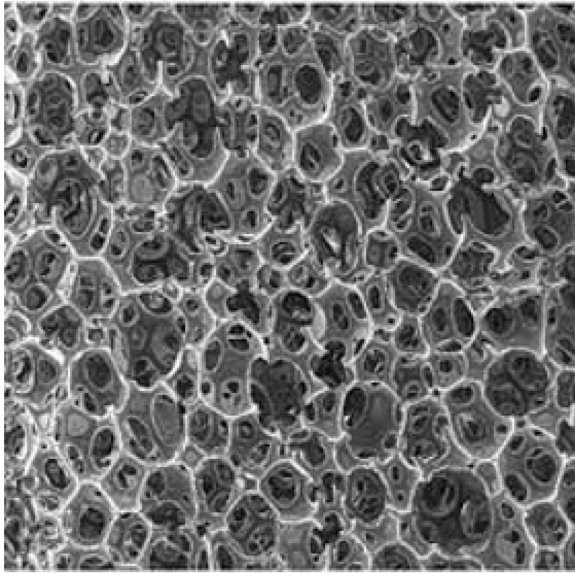
### 1.1. Overview

Currently, various rigid highly porous organic foam materials (hyperfoams) are widely used as shock absorbers due to their ability to attenuate mechanical wave energy [1]; also see Fig. 1a. It was assumed that this attenuation takes place because of two main mechanisms (i) scattering of acoustic waves by pores [2] and (ii) viscoelastic properties of the skeleton material [3]. Meanwhile, theoretical studies based on the two-scale asymptotic analysis testify that waves with wavelengths that are several orders of magnitude larger as compared to the typical pore dimension can hardly be scattered by small pores [4, 5]. Similarly, the considered viscoelastic effects can make a significant impact on multiple loading cycles (e.g., during vibration) [6, 7], but are not able to provide sufficient attenuation for propagating bulk waves, especially single short-duration pulses at sufficiently small distances from the excitation source [8, 9]. Note that a stochastic hyperfoam structure can also be observed in aerogels [10] (Fig. 1b).

The majority of non-porous stitched polymers exhibiting almost no compressibility in a large range of principal stretches, which are actually eigenvalues of the Cauchy–Green strain tensors, are modeled by the non-compressible versions of the Ogden potential [12, 13], Mooney–Rivlin potential [14–18], Yeoh potential [19–21], or Arruda–Boyce potential [22–25]. However, the considered highly porous polymers demonstrate large compressibility with a complicated but monotonic variation of Cauchy stress vs. strain [26–30].

To model highly porous elastic materials, Hill [31] proposed the following potential

$$W(\lambda_1, \lambda_2, \lambda_3) = \sum_{m \in M} \frac{C_m}{|m|} \left( \sum_{k=1}^3 \lambda_k^m - 3 + \frac{1}{|n|} (J^{-mn} - 1) \right), \quad (1.1)$$



(A) Polyurethane (PU) hyperfoam [11]



(B) Aerogel [10]

FIG. 1. Microstructure of typical hyperfoams

where  $\lambda_k$ ,  $k = 1, 2, 3$  are the eigenvalues (principal stretches) of the strain gradient  $\mathbf{F}$ ,  $C_m$  are the experimentally defined coefficients,  $M$  is a finite set of real numbers, and

$$J \equiv \det(\mathbf{F}) = \lambda_1 \lambda_2 \lambda_3. \quad (1.2)$$

With potential 1.1, the principal components of the Cauchy stress tensor become

$$\sigma_i = \lambda_i^{-1} \sum_{m \in M} C_m (\lambda_i^m - J^{-nm}). \quad (1.3)$$

Note that according to [31] neither of the exponents  $m$  or  $n$  need to be positive and integer. Considering uniaxial tension–compression with conditions

$$\lambda_1 = \lambda; \quad \sigma_2 = \sigma_3 = 0 \quad (1.4)$$

and taking into account Eqs. 1.3, Storåkers [32] constructed expressions for the eigenvalues  $\lambda_k$   $k = 2, 3$

$$\lambda_k = \lambda^{-\frac{n}{2n+1}}, \quad k = 2, 3. \quad (1.5)$$

Blatz & Ko [33], analyzing hyperfoams made of polyurethanes, revealed that the general potential 1.1 can be reduced to the following one-parametric form with  $m = -2$  and  $n = 2^{-1}$ , which yields

$$W(\lambda_1, \lambda_2, \lambda_3) = \frac{\mu}{2} \left( \sum_{k=1}^3 \lambda_k^{-2} + 2J - 5 \right). \quad (1.6)$$

Equation 1.5 for the Blatz–Ko potential 1.6 yields

$$\lambda_k = \lambda^{-\frac{1}{4}}, \quad k = 2, 3. \quad (1.7)$$

The apparent non-smooth variation of the potential at  $\lambda \rightarrow 1 \pm 0$  visible in Fig. 2a disappears when moving from the semi-logarithmic scale to the Cartesian scale in Fig. 2b. The plots in Fig. 2 demonstrate the nonlinear behavior of the elastic potential over the whole range of uniaxial stretches  $\lambda \in [0.2; 1.2]$ , ensuring nonlinearity in the stress–stretch relation [27]. It should also be noted that the considered

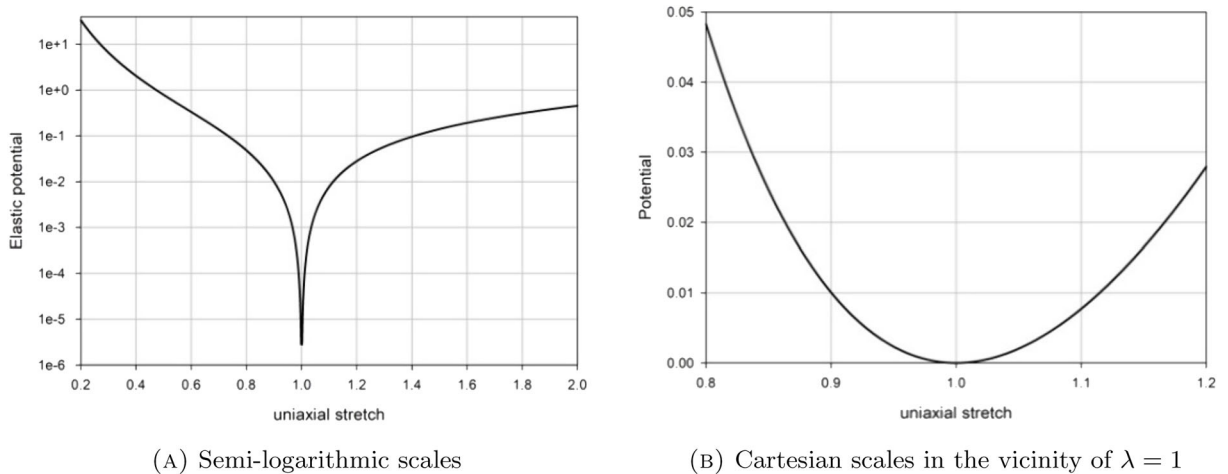


FIG. 2. The Blatz–Ko potential for hyperfoam under uniaxial compression–tension

potential 1.6 along with a more general potential 1.1 is quite often used for modeling different polymeric materials with high porosity [34–37]. Karp and Durban [38] reported a comprehensive analysis of dynamic spectral response of prestressed plates with material behavior given by Blatz–Ko potential.

## 1.2. Problem statement

Herein, uniaxial wave propagation in a hyperfoam rod modeled by the Blatz–Ko potential 1.6 is analyzed, revealing, apparently for the first time, (i) the formation and propagation of (strong) shock wave fronts associated with discontinuities in the strain field; (ii) the attenuation of displacement magnitudes with distance from the excitation source; therefore, (iii) the attenuation of both kinetic and strain energy; and (iv) the simultaneous release of thermal energy. These observations may indicate that the most probable mechanism for the attenuation of waves in a hyperfoam material can be associated with the formation and propagation of shock wave fronts and not the previously assumed viscous properties of the material [39,40], or scattering by micropores [3]. Thus, it is demonstrated that mechanical energy dissipation can be achieved in a purely hyperelastic system without viscous or dry friction properties.

The current analysis is based on solving nonlinear hyperbolic equation for a traveling stress wave in a hyperfoam material modeled by the Blatz–Ko potential 1.6. The solution for the considered hyperbolic equation is constructed by the finite element (FE) method for spatial discretization coupled with an explicit energy-preserving Lax–Wendroff numerical scheme for time integration.

## 2. Governing equations

### 2.1. Cauchy stress, tangent modulus, and rod velocity

The Cauchy principal stress [41] for potential 1.6 and conditions 1.7 takes the form

$$\sigma_1(\lambda) \equiv \partial_\lambda W(\lambda) = \mu \left( \lambda^{\frac{5}{2}} - 1 \right) \lambda^{-3}, \quad (2.1)$$

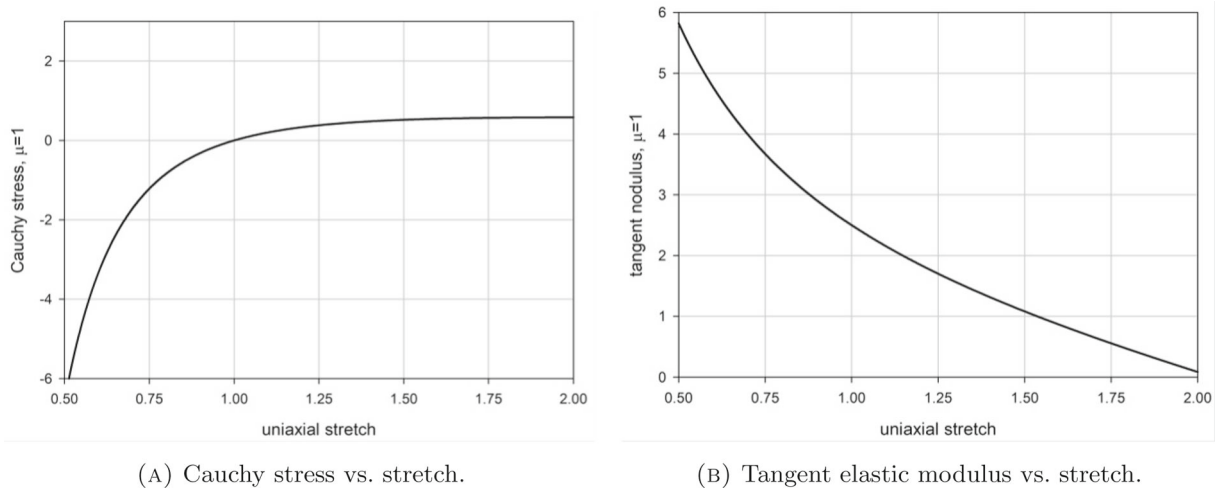


FIG. 3. The Blatz-Ko potential

Hereafter, the subscript at the principal stress will be omitted. Differentiating this principal stress with  $\lambda$  yields the tangent elastic modulus

$$E(\lambda) \equiv \partial_{\lambda} \sigma(\lambda) = \frac{1}{2} \mu \left( 6 - \lambda^{\frac{5}{2}} \right) \lambda^{-4}. \quad (2.2)$$

The material density is defined as [41]

$$\rho(\lambda) \equiv \rho_0 J^{-1} = \rho_0 \lambda^{-\frac{1}{2}}, \quad (2.3)$$

where  $\rho_0$  is the material density at the natural state, assumed to be at  $\lambda = 1$ . Now, following [42–44] and accounting Eqs. 2.2, 2.3 introduce the rod velocity, which is the propagating velocity of an arbitrary stress pulse in a one-dimensional rod

$$c(\lambda) \equiv \sqrt{\frac{E(\lambda)}{\rho(\lambda)}} = \sqrt{\frac{\mu}{2\rho_0} \left( 6 - \lambda^{\frac{5}{2}} \right) \lambda^{-\frac{3}{2}}}. \quad (2.4)$$

*Remark.* The obtained expression 2.2 for tangent elastic modulus is valid for

$$\lambda < 6^{\frac{2}{5}} \approx 2.048, \quad (2.5)$$

from where the Blatz-Ko potential 1.6 becomes non-convex (loses ellipticity). This fact was mentioned and studied in several works [32, 45–50]. Herein, it is assumed that the tensile stretches do not exceed the estimate 2.5. The plots in Fig. 3 show the variation of Cauchy stress and tangent modulus with stretch, varying in the range  $\lambda \in [0.5; 2.0]$ .

## 2.2. Equation of motion

The equation of motion for the considered one-dimensional case can be written in the form [41]

$$\partial_x \sigma(\lambda) = \rho(\lambda) \partial_{tt}^2 u(x, t), \quad (2.6)$$

where  $u(x, t)$  is the displacement field, related to the principal stretch  $\lambda$  of the corresponding diagonal deformation gradient  $\mathbf{F}$

$$\mathbf{F} = \partial_x u(x, t) \mathbf{n} \otimes \mathbf{n} + \mathbf{I} \quad (2.7)$$



FIG. 4. Semi-infinite rod

by the following relation [13]

$$\lambda = 1 + \partial_x u(x, t). \quad (2.8)$$

In Eq. 2.7  $\mathbf{I}$  is the unit  $3 \times 3$ -matrix (tensor), and  $\mathbf{n}$  is the unit vector directed along the axis of the rod.

Now, in view of Eqs. 2.1, 2.2, and 2.8, the desired equation of motion takes the form of a nonlinear hyperbolic equation

$$F(\partial_x u(x, t)) \partial_{xx}^2 u(x, t) = \partial_{tt}^2 u(x, t), \quad (2.9)$$

where

$$F(\partial_x u(x, t)) \equiv \frac{\mu}{2\rho_0} \left( 6 - (1 + \partial_x u(x, t))^{\frac{5}{2}} \right) (1 + \partial_x u(x, t))^{-\frac{3}{2}}. \quad (2.10)$$

### 2.3. Boundary and initial conditions

Consider a semi-infinite rod with a triangle loading applied at the left edge:

$$p(t) = p_0 \begin{cases} 0, & t < 0 \\ t, & 0 < t < t_0 \\ 2t_0 - t, & t_0 < t < 2t_0 \\ 0, & 2t_0 < t \end{cases}, \quad (2.11)$$

where  $2t_0$  is the pulse duration and  $p_0$  is a dimensional constant, specifying the intensity of the applied force load (Fig. 4).

The Sommerfeld attenuation condition [51, 52] is imposed at the right end ( $x \rightarrow \infty$ ):

$$u(x, t)|_{x \rightarrow \infty} = 0; \quad \partial_x u(x, t)|_{x \rightarrow \infty} = 0. \quad (2.12)$$

The initial conditions correspond to the state of rest:

$$u(x, t)|_{t=0} = 0 \quad \partial_t u(x, t)|_{t=0} = 0. \quad (2.13)$$

### 2.4. Equations of energy balance

The equation of energy balance can be written in the form [41]

$$\int_0^t P(\tau) d\tau = E_k + E_s + Q, \quad (2.14)$$

where  $Q$  is the heat release, defined by the release of specific thermal energy, as

$$Q \equiv \int_0^t \int_0^\infty q(x, \tau) dx d\tau. \quad (2.15)$$

In Eq. 2.14  $E_k$  and  $E_s$  are the kinetic and strain energy, respectively

$$E_k = \frac{1}{2} \int_0^\infty \rho(\lambda(x, t)) (\partial_t u(x, t))^2 dx \quad E_s = \frac{1}{2} \int_0^\infty W(\lambda(x, t)) dx, \quad (2.16)$$

and  $P(\tau)$  is the power of external force  $f(\tau)$

$$P(\tau) = f(\tau) \partial_\tau u(0, \tau). \quad (2.17)$$

When shock wave fronts associated with discontinuities in strain appear, Eq. 2.14 needs to be supplemented with a balance equation at the shock wave front [53, 54]

$$\rho_0 V [W] + \frac{1}{2} \rho_0 V [c^2] = -[\sigma c] + [Q], \quad (2.18)$$

where the square brackets denote the jump at the discontinuity and  $V$  is the velocity of the moving shock wave front. Equation 2.18 allows us to define the shock wave velocity:

$$V = \frac{[Q] - [\sigma c]}{\rho_0 [W] + \frac{1}{2} \rho_0 [c^2]}. \quad (2.19)$$

Note that according to [41]

$$c_{\min} < V < c_{\max}, \quad (2.20)$$

where  $c_{\min}$ ,  $c_{\max}$  are the limiting values of particle velocities at both sides of the shock wave fronts.

## 2.5. FE formulation

The governing equations are solved by applying FE method for spatial discretization and the FD method in the time-domain coupled with an explicit Lax–Wendroff energy conservation numerical scheme [51, 55]. To achieve a conditionally stable numerical algorithm, the Courant–Friedrichs–Lewy (CFL) condition is imposed on the time increment  $\Delta t$ , which for the considered problem reads as [56, 57]

$$\Delta t < \Delta t_{CFL} \equiv \frac{\Delta x}{\max_\lambda c(\lambda)}, \quad (2.21)$$

where  $\Delta t_{CFL}$  is the CFL time increment,  $\Delta t$  is the time increment,  $\Delta x$  is the spatial increment (mesh size), and  $c(\lambda)$  is the rod velocity, defined by Eq. 2.4; the principal stretch  $\lambda$  satisfies the convexity condition

$$\partial_{\lambda\lambda}^2 W(\lambda) = \frac{1}{2} \mu \left( 6 - \lambda^{\frac{5}{2}} \right) \lambda^{-4} > 0, \quad (2.22)$$

and, thus,  $\lambda$  should satisfy condition 2.5. In the current analysis, a two-step predictor–corrector form of the Lax–Wendroff scheme is used [51]

$$u(x_{j+1/2}; t_{n+1/2}) = \frac{1}{2} (u(x_{j+1}; t_n) + u(x_j; t_n)) - \frac{\Delta t}{2\Delta x} (F(u(x_{j+1}; t_n)) - F(u(x_j; t_n))), \quad (2.23)$$

where  $x_j$  is a spatial node and  $F$  is the nonlinear function, defined by Eq. 2.10.

The explicit dynamics finite element commercial software ANSYS LS-DYNA [58] was utilized to solve the problem numerically. There was no possibility to utilize simplest two-node linear elements with Blatz–Ko material model in LS-DYNA ® software, so more complicated 2D elements with rotational symmetry were used to simulate wave propagating in the rod (Fig. 4), with a load given by Eq. 2.11. To perform mesh convergence analysis, total number of elements was varied in the range  $7K \leq N \leq 22K$ . The mesh convergence analysis reveals almost identical displacement and stress fields for  $N \geq 10K$ ; hence,  $N \approx 10K$  was chosen for the further computational analysis. Instead of imposing the Sommerfeld attenuation condition 2.12 at  $x \rightarrow \infty$ , the points of observation were chosen in such a way to ensure the absence of reflected waves from the right end of the rod. In the current model, the load at the left end of the rod was defined by Eq. 2.11 with  $t_0 = 30 \mu s$  and  $p_0 = 150 N$ .

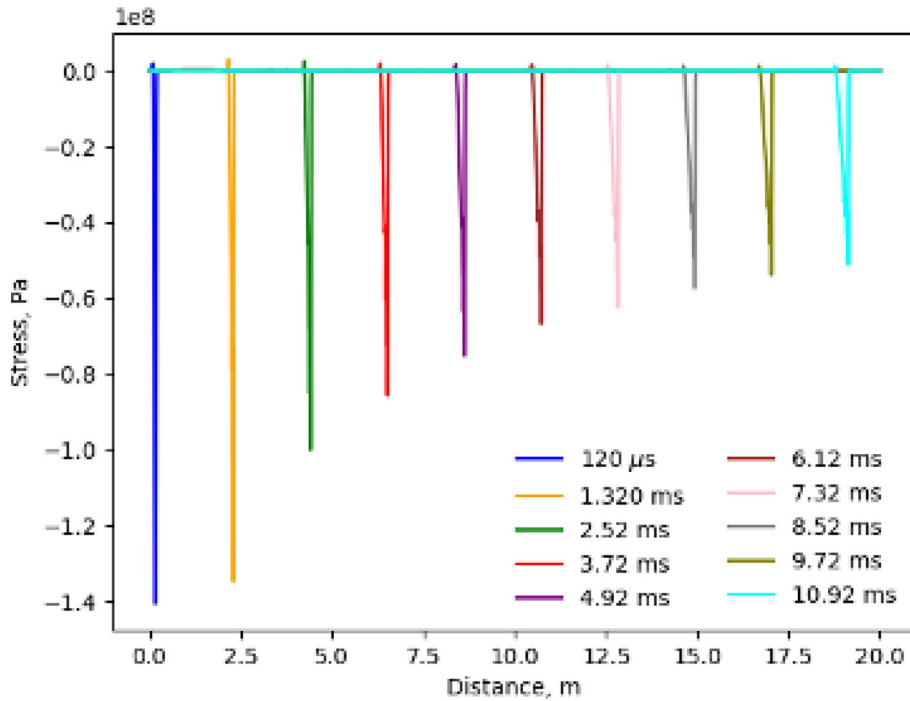


FIG. 5. Compressive load pulse traveling along the rod. Different colors are referred to different times

### 3. Numerical analysis

The force loading shown in Fig. 4 and defined by Eq. 2.11 reveals that the applied delta-like pulse generates the initially triangle pulse propagating with variable velocity dependent upon  $\varepsilon$  by Eq. 2.4. Since the speed of propagation and material density are highly dependent upon strain  $\varepsilon$ , as plots in Fig. 3 show, some parts of the pulse may travel faster than others. These overtakes result in (i) an overlap of the slower moving parts of the leading wave front by the faster moving parts contained inside the pulse; this phenomenon causes the formation of multiple shock wave fronts; (ii) spreading out the initially narrow triangle and its distortion; and (iii) decrease in mechanical energy due the formation and propagation of shock wave fronts, at which the mechanical energy dissipation occurs [53]. All these phenomena are observed at propagating wave pulse in the considered Blatz–Ko rod (see Fig. 5), where the variation of the principal component of the Cauchy stress tensor versus time is plotted. Herein, the Cauchy stress tensor is defined as [41]

$$\sigma = J^{-1} \frac{\partial W}{\partial \mathbf{F}} \cdot \mathbf{F}, \quad (3.1)$$

yielding the desired principal component for  $\sigma$ , and the Lagrangian finite strain tensor

$$\mathbf{E} = \frac{1}{2} (\mathbf{B} - \mathbf{I}). \quad (3.2)$$

The typical stress pulses at the origin ( $t = 120 \mu s$ ) and somewhere in the middle of the rod ( $t = 8.52 ms$ ), where the shock wave front is formed, are given in Fig. 6.

The variation of the pulse stress amplitude versus distance is plotted in Fig. 7, revealing a substantial decrease in the stress amplitudes with distance.

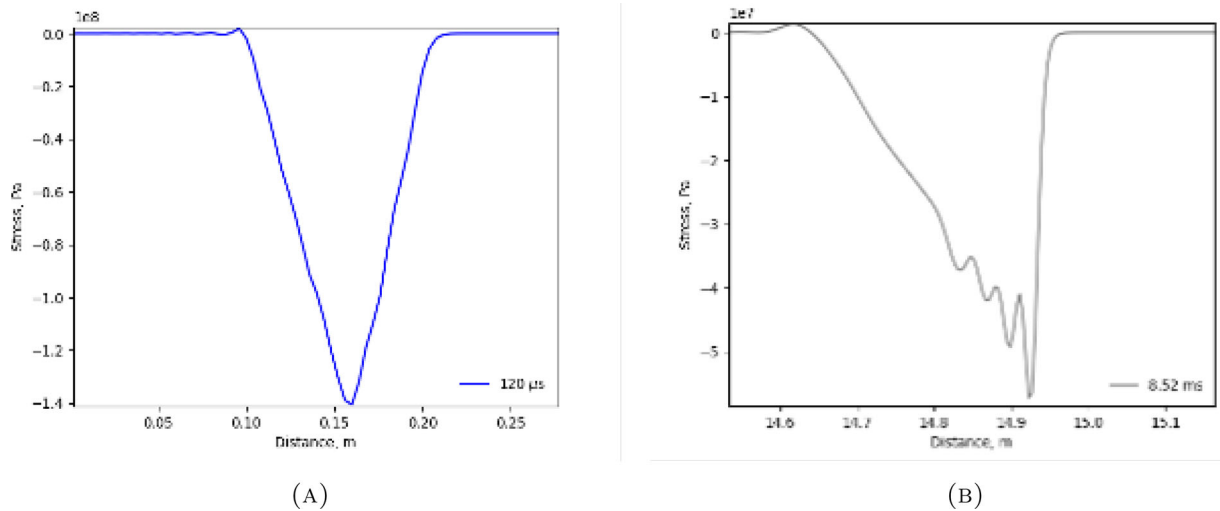


FIG. 6. The compressive wave shape for: a) initial time and b) time when the shock wave front is formed

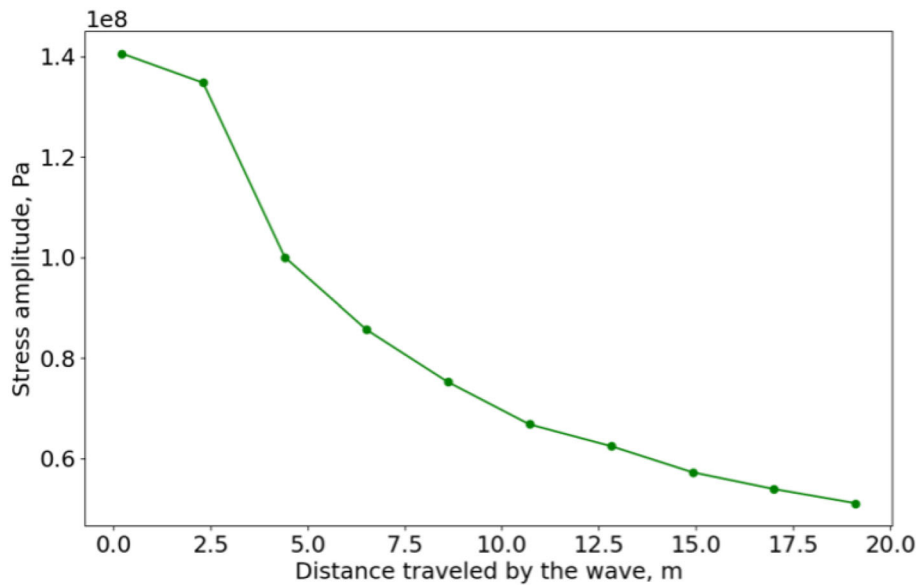


FIG. 7. The amplitude of the stress pulse as a function of distance traveled by the pulse along the rod

It has also been observed that both kinetic and strain energy decrease with time and distance from the left end of the rod, while heat is released in the expense of the losses in mechanical energy.

#### 4. Concluding remarks

Analyzing excitation of the delta-like acoustic waves propagating in a semi-infinite rod modeled by the Blatz–Ko hyperelastic potential, which describes the stress–strain relations of various foams, including



polymer hyperfoams [9] and aerogels [10,30,59], revealed that the elastic tangent modulus (Fig. 3a) varies monotonically with strain in the whole range of admissible values of the principal stretch 2.5, ensuring the convexity of the considered potential. Regarding the propagation of the delta-like pulses along the rod, it has been observed that the Cauchy stress attenuates with the distance (Figs. 5 and 7), caused by the formation and propagation of the shock wave fronts, which appear at the head fronts of the pulses (Fig. 6). Moreover, the performed analysis also revealed that both kinetic and strain energy dissipate resulting in the significant thermal energy release. Cohen and Durban [60] proposed a theoretical framework for the propagation of longitudinal shock waves in elastoplastic solids, utilizing an analogy to the piston-driven shock tube model commonly employed in fluid dynamics. This formulation was subsequently extended to account for steady shock waves in porous elastoplastic media [61]. The findings from these studies elucidate an additional dissipation mechanism for shock wave energy, namely plastic deformation within the solid matrix. Thus, apparently for the first time, the loss of mechanical energy is observed at the propagation of acoustic waves in a purely mechanical system, modeled by the Blatz–Ko potential, ensuring a continuous and smooth variation of mechanical properties. This phenomenon reveals a possibility for the mechanical wave attenuation due to the formation and propagation of the shock wave fronts.

## Declarations

**Conflict of interest** The authors declare that they have no conflict of interest.

**Open Access.** This article is licensed under a Creative Commons Attribution 4.0 International License, which permits use, sharing, adaptation, distribution and reproduction in any medium or format, as long as you give appropriate credit to the original author(s) and the source, provide a link to the Creative Commons licence, and indicate if changes were made. The images or other third party material in this article are included in the article's Creative Commons licence, unless indicated otherwise in a credit line to the material. If material is not included in the article's Creative Commons licence and your intended use is not permitted by statutory regulation or exceeds the permitted use, you will need to obtain permission directly from the copyright holder. To view a copy of this licence, visit <http://creativecommons.org/licenses/by/4.0/>.

**Publisher's Note** Springer Nature remains neutral with regard to jurisdictional claims in published maps and institutional affiliations.

## References

- [1] Hakan, U., Ipek, B.: Dynamic characterization and modeling of rubber shock absorbers: A comprehensive case study. *J. Low Freq. Noise Vibr. Active Control* **37**(3), 146134841772595 (2018)
- [2] Das, G., Chakraborty, R.: Effect of porosity on wave scattering by a vertical porous barrier over a rectangular trench. *J. Marine Sci. Appl.* **23**, 85–100 (2024)
- [3] Friend, N.M., Kren, A.P.: Determination of the viscoelastic properties of elastomeric materials by the dynamic indentation method. *Polym. Test.* **23**, 369–375 (2004)
- [4] Bensoussan, A., Lions, J.L.: *Asymptotic Analysis for Periodic Structures*. North Holland, Amsterdam (1978)
- [5] Allaire, G.: Homogenization and two-scale convergence. *SIAM J. Math. Anal.* **23**(6), 1482–1518 (1992)
- [6] Brown, R.: *Physical Testing of Rubber*. Springer, New York (2006)
- [7] Goldstein, R.V., et al.: The modified Cam-Clay (MCC) model: cyclic kinematic deviatoric loading. *Arch. Appl. Mech.* **86**(12), 2021–2031 (2016)
- [8] Carcione, J.M., Kosloff, D., Kosloff, R.: Wave propagation simulation in a linear viscoelastic medium. *Geophys. J. Int.* **95**, 597–611 (1988)
- [9] Berjamine, H., Destrade, M., Saccomandi, G.: Singular travelling waves in soft viscoelastic solids of rate type. *Eur. J. Mech. A* **103**, 105144 (2024)
- [10] Lyu, Sh., et al.: Effect of high temperature on compression property and deformation recovery of ceramic fiber reinforced silica aerogel composites. *Sci. China Technol. Sci.* **60**(11), 1681–1691 (2017)
- [11] Bashirzadeh, R., Gharehbaghi, A.: An investigation on reactivity, mechanical and fire properties of PU flexible foam. *J. Cellular Plast.* **46**(2), 129–158 (2010)
- [12] Ogden, R.W.: Waves in isotropic elastic materials of Hadamard, Green, or harmonic type. *J. Mech. Phys. Solids* **18**(2), 149–163 (1970)

- [13] Ogden, R.W.: *Nonlinear Elastic Deformations*. Dover Publications, New York (1984)
- [14] Murphy, J.G.: Strain energy functions for a Poisson power law function in simple tension of compressible hyperelastic materials. *J. Elast.* **60**, 151–164 (2000)
- [15] Boulanger, P., Hayes, M.A.: Finite amplitude waves in Mooney-Rivlin and Hadamard materials. In: *Topics in Finite Elasticity*, eds. Hayes, M.A., Saccomandi, G., Springer, Wien (2001)
- [16] Treloar, L.R.G.: *The Physics of Rubber Elasticity*. Oxford University Press, Oxford (2005)
- [17] Hamza, M., Hassan, A.: Hyperelastic constitutive modeling of rubber and rubber-like materials under finite strain. *Eng. Tech. J.* **28**(13), 2560–2575 (2010)
- [18] Chen, J., Garcia, E.S., Zimmerman, S.C.: Intramolecularly cross-linked polymers: From structure to function with applications as artificial antibodies and artificial enzymes. *Acc. Chem. Res.* **53**(6), 1244–1256 (2020)
- [19] Yeoh, O.H.: Some forms of the strain energy function for rubber. *Rubber Chem. Technol.* **66**(5), 754–771 (1993)
- [20] Gajewski, M., Szczerba, R., Jemioło, S.: Modelling of elastomeric bearings with application of Yeoh hyperelastic material model. *Procedia Eng.* **111**, 220–227 (2015)
- [21] Pence, T.J., Gou, K.: On compressible versions of the incompressible neo-Hookean material. *Math. Mech. Solids* **20**(2), 157–182 (2015)
- [22] Arruda, E.M., Boyce, M.C.: A three-dimensional model for the large stretch behavior of rubber elastic materials. *J. Mech. Phys. Solids* **41**(2), 389–412 (1993)
- [23] Boyce, M.C.: Direct comparison of the Gent and the Arruda-Boyce constitutive models for rubber elasticity. *Rubber Chem. Technol.* **69**, 781–785 (1996)
- [24] Boyce, M.C., Arruda, E.M.: Constitutive models of rubber elasticity: A review. *Rubber Chem. Technol.* **73**(3), 504–523 (2000)
- [25] Bergstrom, J.S., Boyce, M.C.: Deformation of elastomeric networks: Relation between molecular level deformation and classical statistical mechanics models of rubber elasticity. *Macromolecules* **34**(3), 614–626 (2001)
- [26] Beatty, M.F.: Topics in finite elasticity: hyperelasticity of rubber, elastomers, and biological tissues-with examples. *Appl. Mech. Rev.* **40**(12), 1699–1734 (1987)
- [27] Parmeneter, K.E., Milstein, F.: Mechanical properties of silica aerogels. *J. Non-Crystalline Solids* **223**(3), 179–189 (1998)
- [28] Landauer, A., et al.: Experimental characterization and hyperelastic constitutive modeling of open-cell elastomeric foams. *J. Mech. Phys. Solids* **133**, 103701 (2019)
- [29] Bresler, F.H., Muller, J.H., Venter, G.: Investigating an inverse Finite Element approach for characterising soft materials. *R&D J.* **37**, 80–88 (2021)
- [30] Patil, S.P., et al.: Mechanical modeling and simulation of aerogels: A review. *Ceram. Int.* **47**, 2981–2998 (2021)
- [31] Hill, R.: Aspects of invariance in solid mechanics. *Adv. Appl. Mech.* **18**, 1–72 (1978)
- [32] Storåkers, B.: On material representation and constitutive branching in finite compressible elasticity. *J. Mech. Phys. Solids* **34**(2), 125–145 (1986)
- [33] Blatz, P.D., Ko, W.L.: Application of finite elasticity to the deformation of rubbery materials. *Trans. Soc. Rheol.* **6**, 223–251 (1962)
- [34] Kakavas, P.A.: Influence of the cavitation on the stress-strain fields of compressible Blatz-Ko materials at finite deformation. *Int. J. Solids Struct.* **39**, 783–795 (2002)
- [35] Peyraut, F.: Loading restrictions for the Blatz-Ko hyperelastic model-application to a finite element analysis. *Int. J. Non-Linear Mech.* **39**, 969–976 (2004)
- [36] Hadoush, A.: Effect of Poisson's ratio on internally balanced Blatz-Ko material model. *Acta Mech. Sinica* **39**, 422350 (2023)
- [37] Bozkurt, M.O., Tagarielli, V.L.: A data-driven constitutive model for porous elastomers at large strains. *Extr. Mech. Lett.* **70**, 102170 (2024)
- [38] Karp, B., Durban, D.: Evanescent and propagating waves in prestretched hyperelastic plates. *Int. J. Solids Struct.* **42**, 1613–1647 (2005)
- [39] Li, S., et al.: Explicit/implicit multi-time step co-simulation in unbounded medium with Rayleigh damping and application for wave barrier. *Eur. J. Environ. Civil Eng.* **24**(14), 2400–2421 (2020)
- [40] Li, S., et al.: Benchmark for three-dimensional explicit asynchronous absorbing layers for ground wave propagation and wave barriers. *Comput. Geotech.* **131**, 103808 (2021)
- [41] Truesdell, C., Noll, W.: *The Non-Linear Field Theories of Mechanics*, 3rd edn. Springer, Berlin (2004)
- [42] Kolsky, H.: Stress waves in solids. *J. Sound Vib.* **1**, 88–110 (1964)
- [43] Ilyashenko, A.V., et al.: Theoretical aspects of applying Lamb waves in nondestructive testing of anisotropic media. *Russ. J. Nondestruct. Test.* **53**, 243–259 (2017)
- [44] Ilyashenko, A.V., et al.: Pochhammer-Chree waves: polarization of the axially symmetric modes. *Arch. Appl. Mech.* **88**, 1385–1394 (2018)
- [45] Knowles, J.K., Sternberg, E.: On the singularity induced by certain mixed boundary conditions in linearized and nonlinear elastostatics. *Int. J. Solids Struct.* **11**, 1173–1201 (1975)

- [46] Knowles, J.K., Sternberg, E.: On the failure of ellipticity and the emergence of discontinuous deformation gradients in plane finite elastostatics. *J. Elasticity* **8**, 329–379 (1978)
- [47] Thompson, J.M.T., Shorrock, P.A.: Bifurcational instability of an atomic lattice. *J. Mech. Phys. Solids* **23**, 21–37 (1975)
- [48] Kuznetsov, S.V.: “Forbidden” planes for Rayleigh waves. *Quart. Appl. Math.* **60**(1), 87–97 (2002)
- [49] Kuznetsov, S.V.: Love waves in stratified monoclinic media. *Quart. Appl. Math.* **62**(4), 749–766 (2004)
- [50] Li, S., et al.: Hybrid asynchronous absorbing layers based on Kosloff damping for seismic wave propagation in unbounded domains. *Comput. Geotech.* **109**, 69–81 (2019)
- [51] Belytschko, T., Liu, W.K., Moran, B.: *Nonlinear Finite Elements for Continua and Structures*. Wiley, N.Y. (2000)
- [52] Terentjeva, E.O., et al.: Planar internal Lamb problem: Waves in the epicentral zone of a vertical power source. *Acoust. Phys.* **61**, 356–367 (2015)
- [53] Truesdell, C.: General and exact theory of waves in finite elastic strain. *Arch. Ration. Mech. Anal.* **8**, 263–296 (1961)
- [54] Bland, D.R.: On shock structure in a solid. *J. Inst. Math. Appl.* **1**, 56–75 (1965)
- [55] Lax, P.D., Wendroff, B.: Difference schemes for hyperbolic equations with high order of accuracy. *Commun. Pure Appl. Math.* **17**, 381–398 (1964)
- [56] Scovazzi, G., Song, T., Zeng, X.: A velocity/stress mixed stabilized nodal finite element for elastodynamics: Analysis and computations with strongly and weakly enforced boundary conditions. *Comput. Methods Appl. Mech. Eng.* **325**(1), 532–576 (2017)
- [57] Winnicki, I., Jasinski, J., Pietrek, S.: New approach to the Lax-Wendroff modified differential equation for linear and nonlinear advection. *Numer. Meth. Part. Differ. Eq.* **35**, 2275–2304 (2019)
- [58] ANSYS Inc.: ANSYS LS-DYNA simulation software. (2024). <https://lsdyna.ansys.com>
- [59] Guild, M.D., et al.: Aerogel as a soft acoustic metamaterial for airborne sound. *Phys. Rev. Appl.* **5**, 034012 (2016)
- [60] Cohen, T., Durban, D.: Longitudinal shock waves in solids: the piston shock analogue. *Proc. R. Soc. A.* **470**, 20130061 (2014)
- [61] Cohen, T., Durban, D.: Steady shock waves in porous plastic solids. *Int. J. Solids Struct.* **71**, 70–78 (2015)

Vladimir Bratov  
Edinburgh Napier University  
Edinburgh  
UK  
e-mail: v.bratov@napier.ac.uk

Sergey V. Kuznetsov  
Moscow State University of Civil Engineering  
Moscow  
Russia  
e-mail: kuzn-sergey@yandex.ru

(Received: March 20, 2025; revised: April 25, 2025; accepted: May 12, 2025)

## Terms and Conditions

Springer Nature journal content, brought to you courtesy of Springer Nature Customer Service Center GmbH (“Springer Nature”). Springer Nature supports a reasonable amount of sharing of research papers by authors, subscribers and authorised users (“Users”), for small-scale personal, non-commercial use provided that all copyright, trade and service marks and other proprietary notices are maintained. By accessing, sharing, receiving or otherwise using the Springer Nature journal content you agree to these terms of use (“Terms”). For these purposes, Springer Nature considers academic use (by researchers and students) to be non-commercial.

These Terms are supplementary and will apply in addition to any applicable website terms and conditions, a relevant site licence or a personal subscription. These Terms will prevail over any conflict or ambiguity with regards to the relevant terms, a site licence or a personal subscription (to the extent of the conflict or ambiguity only). For Creative Commons-licensed articles, the terms of the Creative Commons license used will apply.

We collect and use personal data to provide access to the Springer Nature journal content. We may also use these personal data internally within ResearchGate and Springer Nature and as agreed share it, in an anonymised way, for purposes of tracking, analysis and reporting. We will not otherwise disclose your personal data outside the ResearchGate or the Springer Nature group of companies unless we have your permission as detailed in the Privacy Policy.

While Users may use the Springer Nature journal content for small scale, personal non-commercial use, it is important to note that Users may not:

1. use such content for the purpose of providing other users with access on a regular or large scale basis or as a means to circumvent access control;
2. use such content where to do so would be considered a criminal or statutory offence in any jurisdiction, or gives rise to civil liability, or is otherwise unlawful;
3. falsely or misleadingly imply or suggest endorsement, approval, sponsorship, or association unless explicitly agreed to by Springer Nature in writing;
4. use bots or other automated methods to access the content or redirect messages
5. override any security feature or exclusionary protocol; or
6. share the content in order to create substitute for Springer Nature products or services or a systematic database of Springer Nature journal content.

In line with the restriction against commercial use, Springer Nature does not permit the creation of a product or service that creates revenue, royalties, rent or income from our content or its inclusion as part of a paid for service or for other commercial gain. Springer Nature journal content cannot be used for inter-library loans and librarians may not upload Springer Nature journal content on a large scale into their, or any other, institutional repository.

These terms of use are reviewed regularly and may be amended at any time. Springer Nature is not obligated to publish any information or content on this website and may remove it or features or functionality at our sole discretion, at any time with or without notice. Springer Nature may revoke this licence to you at any time and remove access to any copies of the Springer Nature journal content which have been saved.

To the fullest extent permitted by law, Springer Nature makes no warranties, representations or guarantees to Users, either express or implied with respect to the Springer nature journal content and all parties disclaim and waive any implied warranties or warranties imposed by law, including merchantability or fitness for any particular purpose.

Please note that these rights do not automatically extend to content, data or other material published by Springer Nature that may be licensed from third parties.

If you would like to use or distribute our Springer Nature journal content to a wider audience or on a regular basis or in any other manner not expressly permitted by these Terms, please contact Springer Nature at

[onlineservice@springernature.com](mailto:onlineservice@springernature.com)